Supporting Information

Azo compounds as a new family of organic electrode materials for alkali-ion batteries

Chao Luo[1], Oleg Borodin[2], Xiao Ji[1,3], Singyuk Hou[1], Karen J. Gaskell[4], Xiulin Fan[1], Ji Chen[1], Tao Deng[1], Ruixing Wang[4], Jianjun Jiang[3], Chunsheng Wang[1]*

[1]Department of Chemical and Biomolecular Engineering, University of Maryland, College Park, Maryland 20742, USA

[2]Electrochemistry Branch, Sensors and Electron Devices Directorate, US Army Research Laboratory, 2800 Powder Mill Rd., Adelphi, MD, 20783, USA

[3]School of Optical and Electronic Information, Huazhong University of Science and Technology, Wuhan, Hubei, 430074, China

[4]Department of Chemistry and Biochemistry, University of Maryland, College Park, Maryland 20742, USA

Corresponding author: cswang@umd.edu

DFT Calculation

Three types of DFT calculations were performed: 1) cluster calculations of AB and ADALS clusters surrounded by implicit solvent represented using SMD(ether) solvation model as implemented in Gaussian package(1); 2) periodic calculations of Li_2ADA, Li_3ADA and Li_4ADA crystals to predict Li intercalation potentials using cp2k package; and 3) periodic calculations of AB and Li_2ADA molecules using VASP to estimate HOMO - LUMO.

1. Cluster calculations were performed on the AB, $(AB)_3$, Li_2ADA, Li_3ADA, Li_4ADA and $(Li_2ADA)_4$ using Gaussian g09 rev. c and g16 rev. a.03 packages(1,2); M05-2X density functional was used as it was shown to accurately describe electron affinity (EA) and ionization potential (IP)(3). M05-2X was found to adequately represent the localized hole in solvent oxidation while B3LYP yielded a delocalized hole(4). The 6-31+G(d,p) basis set was used for most calculations, while a much larger aug-cc-pvTz basis set was used for the few predictions of Raman spectra to investigate the influence of the basis set size on Raman spectra. The SMD implicit solvation model(5) using DiethylEther: dielectric constant ε=4.2400 parameters was used as implemented in g16 package for Raman and redox calculations. The SMD model using dielectric constant of 20 was used for estimating reduction potentials of electrolyte components in the EC:DEC/$LiPF_6$ electrolyte.

The absolute reduction potential of a complex M relative to an electron at rest in vacuum, ($E^0_{abs}(M)$) $E^0_{abs}(M) = -[\Delta G_e + \Delta G^0_S(M^-) - \Delta G^0_S(M)]/F$,

where ΔG_e is the electron affinity in gas-phase at 298.15 K. $\Delta G_S(M^+)$ and $\Delta G_S(M)$ are the free energies of solvation of the reduced and initial complexes M^- and M, respectively; and F is the Faraday constant. $E^0_{abs}(M)$ is related to the Li/Li^+ scale by subtracting 1.4 V as discussed elsewhere(6,7).

2. Intercalation potential calculations using DFT. DFT calculations were performed with the Li_2ADA, Li_3ADA and Li_4ADA crystals containing four ADA molecules per simulation cell. The QUICKSTEP module of the CP2K code with the dual Gaussian and Plane Waves (GPW) method was used(8,9). Valence electrons are described by an atom-centered Gaussian double-zeta basis set augmented with a set of d-type or p-type polarization functions (DZVP-MOLOPT-SR-GTH) with core electrons described by norm-conserving Goedecker-Teter-Hutter (GTH) pseudopotentials(10,11). The gamma point supercell approach was used in combination with 3-dimensioanl Periodic Boundary Conditions (PBC). Calculations were performed using the spin-polarized Perdew-Burke-Ernzerhof (PBE) exchange correlation functional with Grimme's D3 dispersion correction(12,13). The auxiliary planewave basis set energy cutoff of 600 Ry was used. The SCF energy convergence was set to 10^{-6} atomic units(14). For all cell optimization the maximum force was set to 10^{-3} Hartree/Bohr.

Short Born-Oppenheimer molecular dynamics (BOMD) simulations were also performed to equilibrate Li_2ADA, Li_3ADA and Li_4ADA crystals at 800 K and 1000 K for 5-9 ps in order to create additional initial geometries for geometry optimization and assist in finding the most stable packing. The CSVR thermostat with a 50-fs time constant was used(15). MD simulations with time step of 0.5 fs was used. A deuterium mass was used for all hydrogen atoms. Runs were performed using NPT_F flexible cell constant stress tensor ensemble.

To quantify the thermodynamic driving force, the Gibbs free energy ΔG for the reactions are described as

$$\Delta G = E(\mathrm{Li}_{x1}\mathrm{AZO}) - E(\mathrm{Li}_{x2}\mathrm{AZO}) - (x1 - x2) \cdot \mu_{Li}$$

Where $E(\mathrm{Li}_{x1}\mathrm{AZO})$ and $E(\mathrm{Li}_{x2}\mathrm{AZO})$ are the energies of the Li_{x1}AZO and Li_{x2}AZO, respectively; $x1 - x2$ is the change of the number of Li involved reaction; μ_{Li} is the chemical potential of Lithium metal. According to the Nernst equation, the equilibria voltage is calculated as

$$\mathrm{E} = -\frac{\Delta G}{(x1 - x2) \cdot F}$$

for the lithiation from Li_2ADA to Li_3ADA and from Li_3ADA to Li_4ADA.

3. First-principles calculations are performed using VASP code based on DFT(16-18). The ion-electron interaction is described with the Projector Augmented Wave (PAW) method, and the exchange-correlation energy is calculated using general gradient approximation (GGA) with the Perdew-Burke-Ernzerhof (PBE) exchange-correlation functional(19-21). The convergence condition for the energy is 10^{-5} eV, and the structures are relaxed until the force on each atom is less than 0.005 eV/Å. To calculate the LUMO and HOMO, a vacuum larger than 15 Å is used to simulate the molecules(22). In addition, the LUMO and HOMO are visualized using Molekel software(23).

Fig. S1. The dissolution test for AB in commercial carbonated-based electrolyte. The solution in the left represents pure electrolyte, while the solution in the right represents AB/MRSS in the electrolyte.

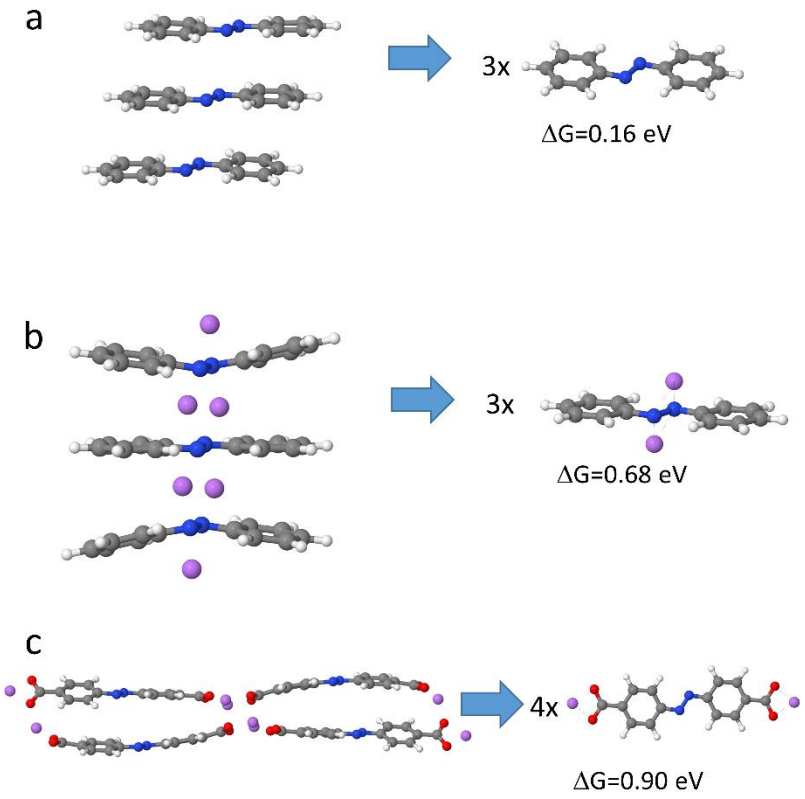

Fig. S2. Dissolution free energies per solvent molecule obtained from DFT calculations using M05-2X function with 6-31+G(d,p) basis set. All complexes were immersed in implicit solvent that was modelled using solvation model SMD(ether) parameters as implemented in g16 Gaussian software.

Fig. S3. The dissolution test for MRSS in commercial carbonated-based electrolyte. The solution in the left represents pure electrolyte, while the solution in the right represents AB/MRSS in the electrolyte.

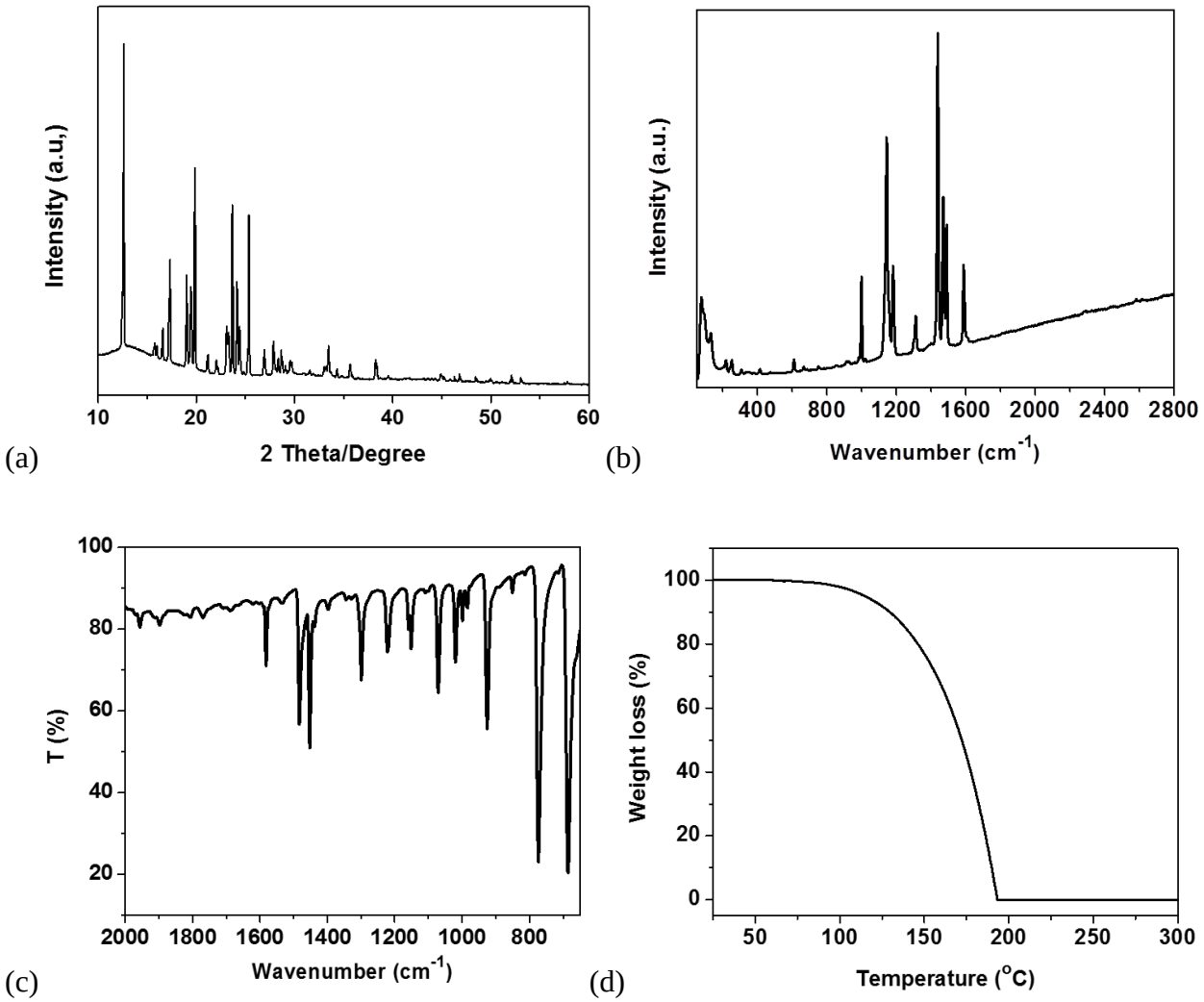

Fig. S4. Material characterization for AB. (a) XRD pattern; (b) Raman spectrum; (c) FTIR spectrum; (d) TG analysis.

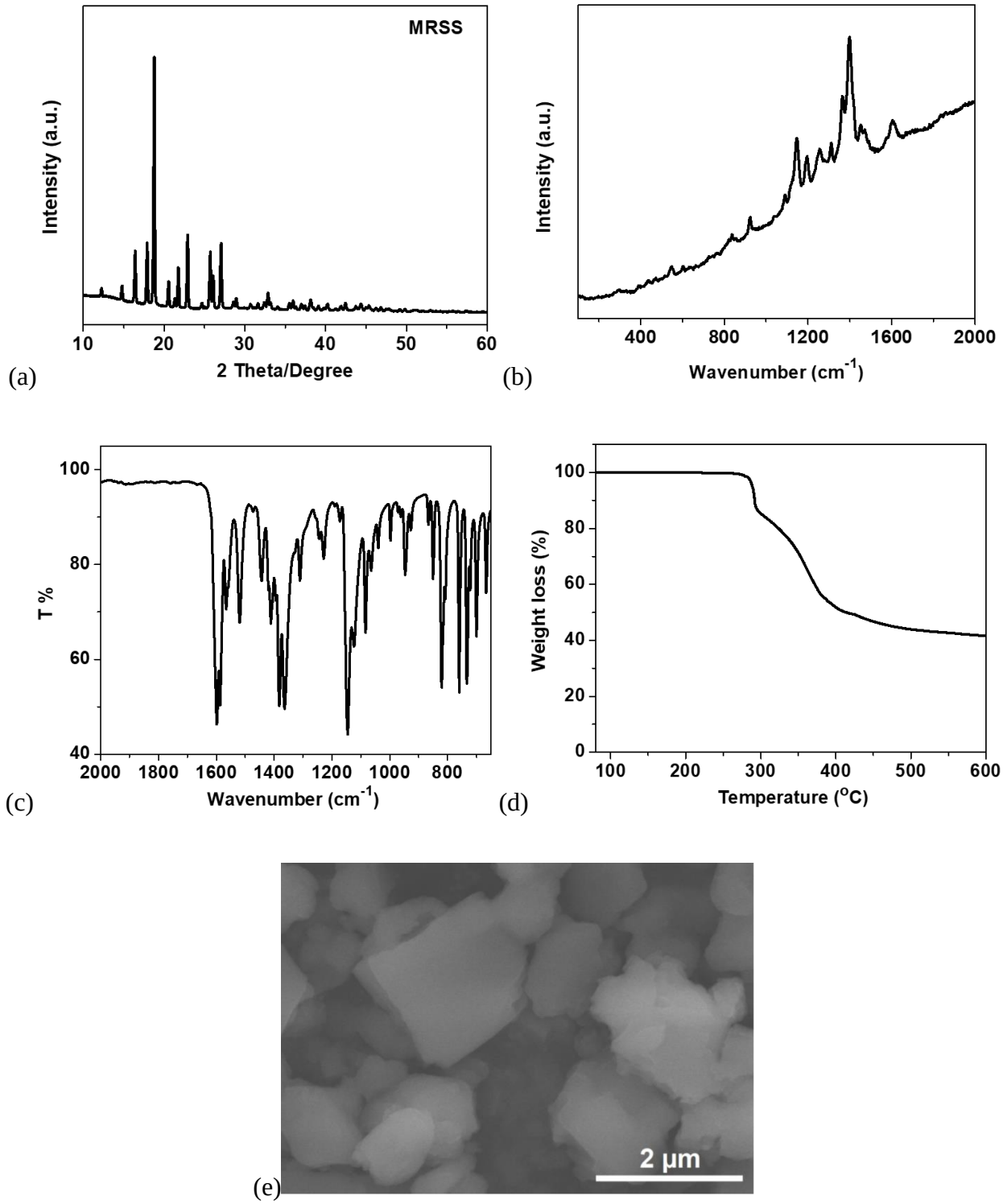

Fig. S5. Material characterization for MRSS. (a) XRD pattern; (b) Raman spectrum; (c) FTIR spectrum; (d) TG analysis; (e) SEM image.

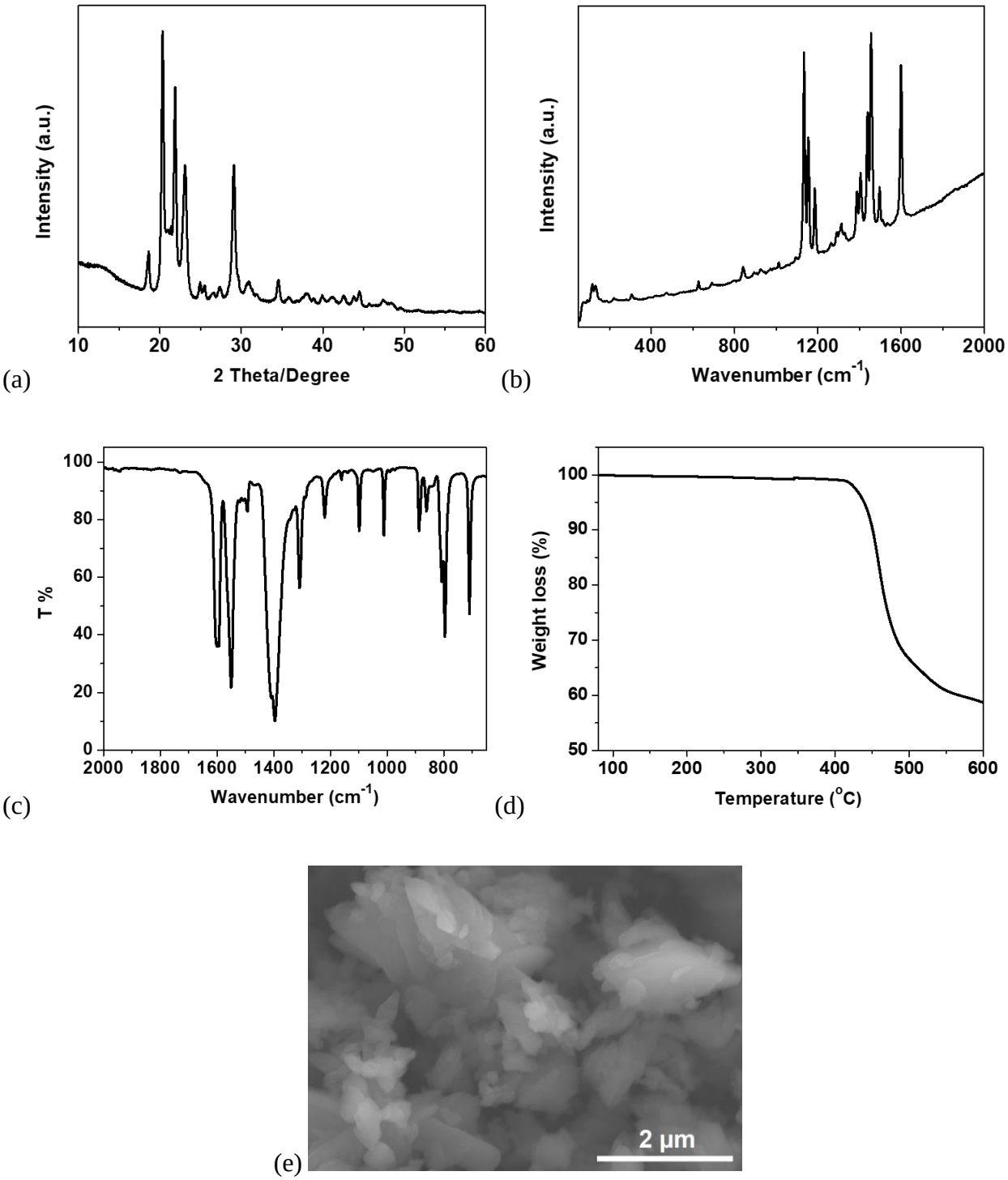

Fig. S6. Material characterization for ADALS. (a) XRD pattern; (b) Raman spectrum; (c) FTIR spectrum; (d) TG analysis; (e) SEM image.

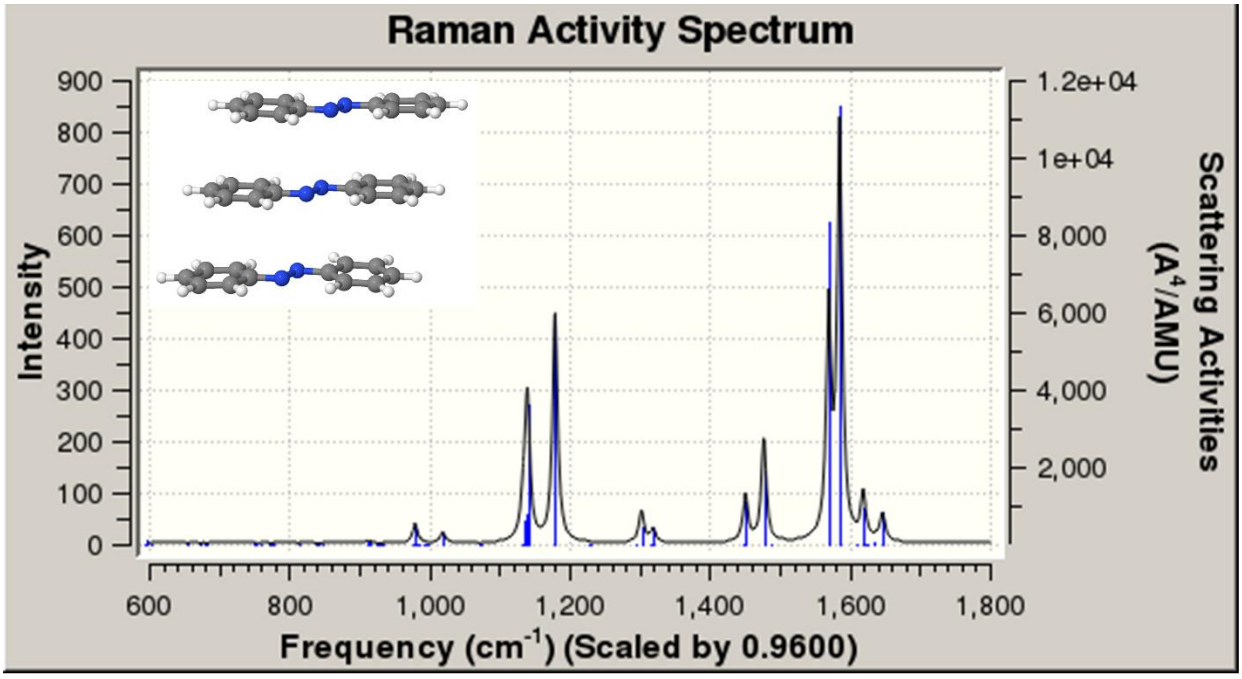

Fig. S7. Raman spectra from DFT calculations of (AB)3 using M05-2X/6-31+G(d,p) and SMD(ether). Frequencies were scaled by 0.96 to match experimental data.

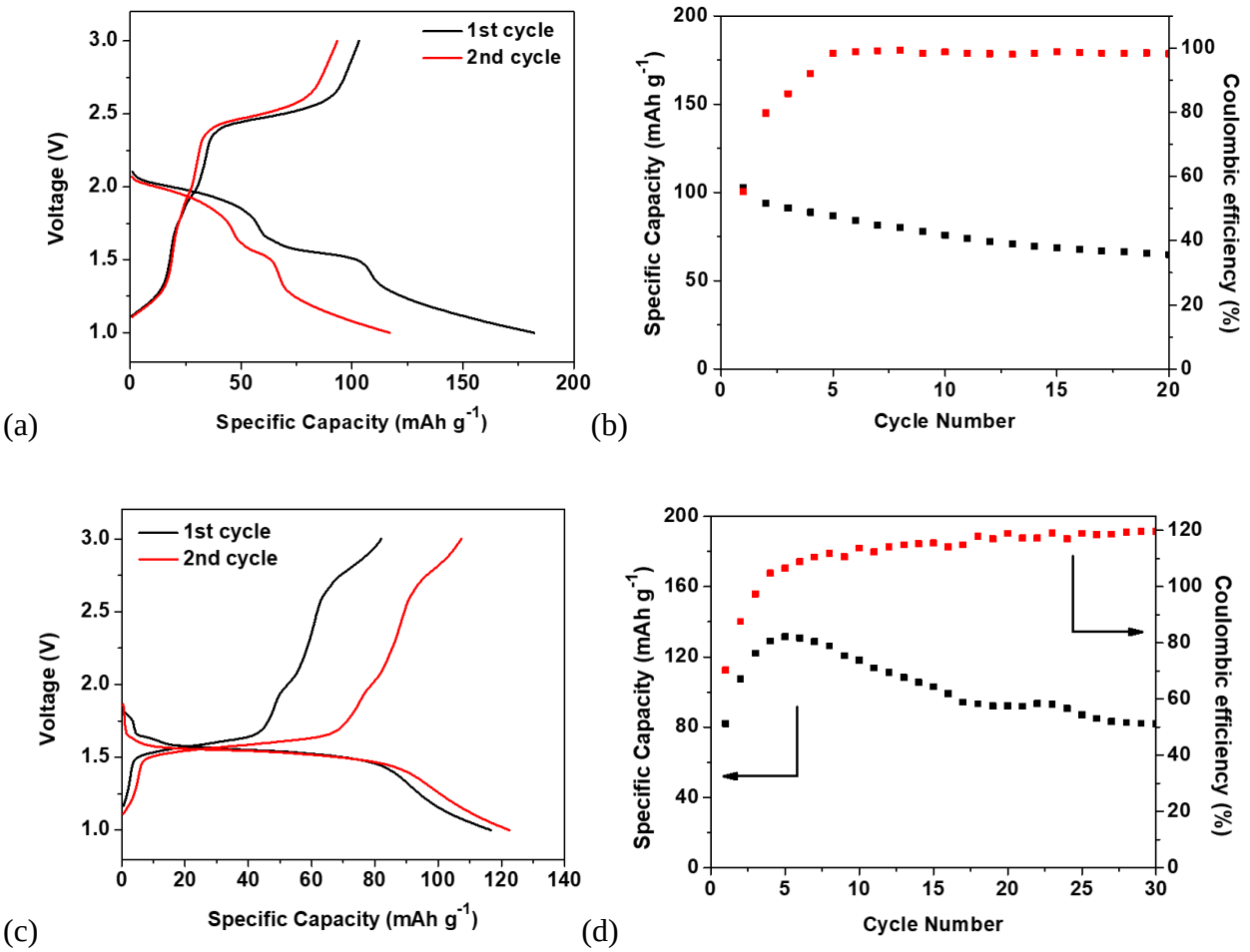

Fig. S8. (a) The galvanostatic charge-discharge curves for AB between 1.0 and 3.0 V versus Li/Li^+; (b) Delithiation capacity and Coulombic efficiency versus cycle number for AB at the current density of 0.5 C; (c) The galvanostatic charge-discharge curves for MRSS between 1.0 and 3.0 V versus Li/Li^+; (d) Delithiation capacity and Coulombic efficiency versus cycle number for MRSS at the current density of 0.5 C.

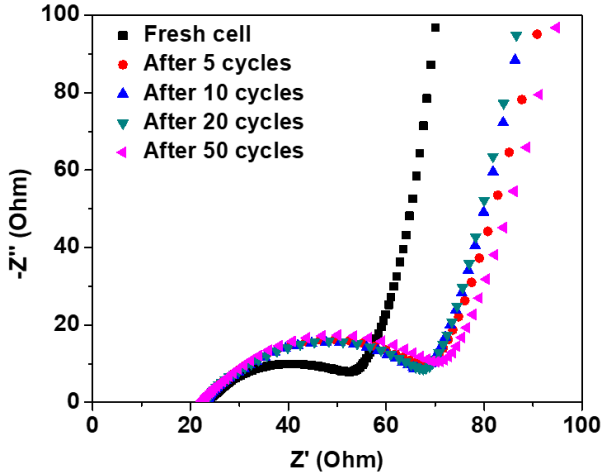

Fig. S9. Nyquist plots for ADALS cells obtained by electrochemical impedance spectroscopy tests before and after cycling at fully charged states.

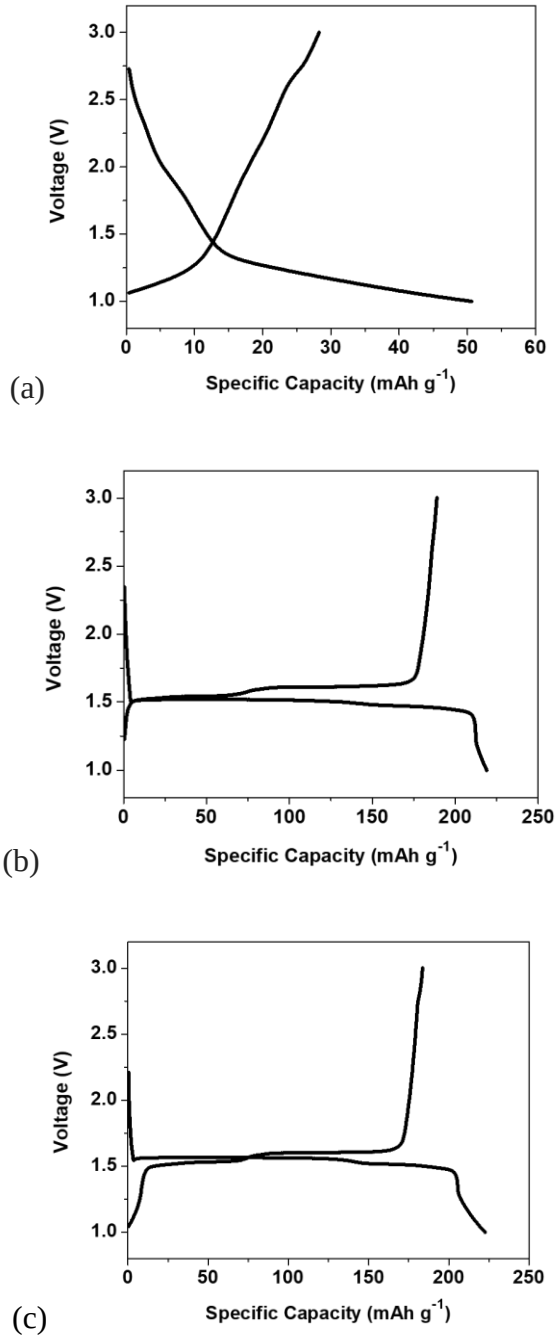

Fig. S10. Electrochemical behaviors of carbon black and ADALS. (a) The first cycle charge-discharge curves of carbon black in 1M $LiPF_6$-EC/DEC electrolyte; (b) The first cycle charge-discharge curves of ADALS electrode with 15 wt% carbon black in 1M $LiPF_6$-EC/DEC electrolyte; (c) The first cycle charge-discharge curves of ADALS electrode in 1M LiTFSI-DOL/DME electrolyte.

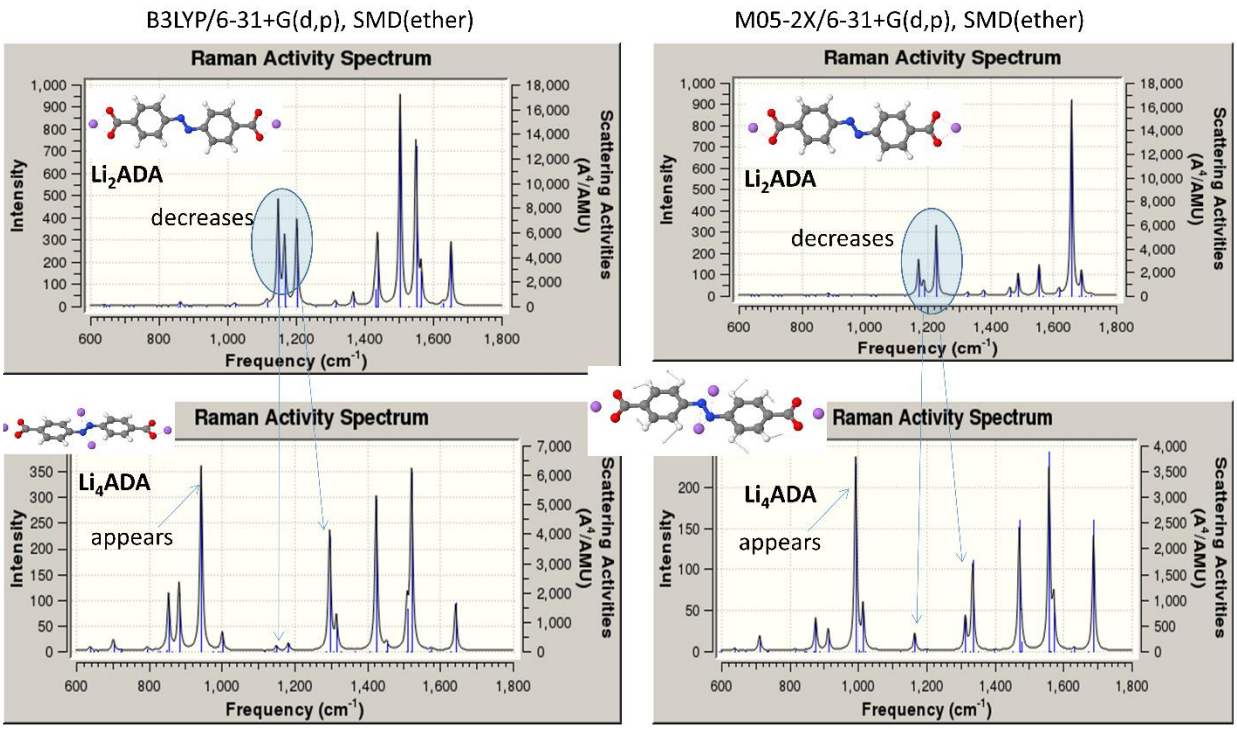

Fig. S11. Raman spectra from DFT calculations of Li_2ADA and Li_4ADA using two functionals B3LYP and M05-2X. The Li-N-N-Li bond gives rise to peaks around 1000 cm^{-1} and 1300 cm^{-1} that were experimentally used in the cycled ADALS at 1 V as shown in Fig. 4b. The peaks around 1200 cm^{-1} are present only in Li_2ADA and experimentally observed only in the pristine ADALS and ADALS cycled at 3 V as shown in Fig. 4b.

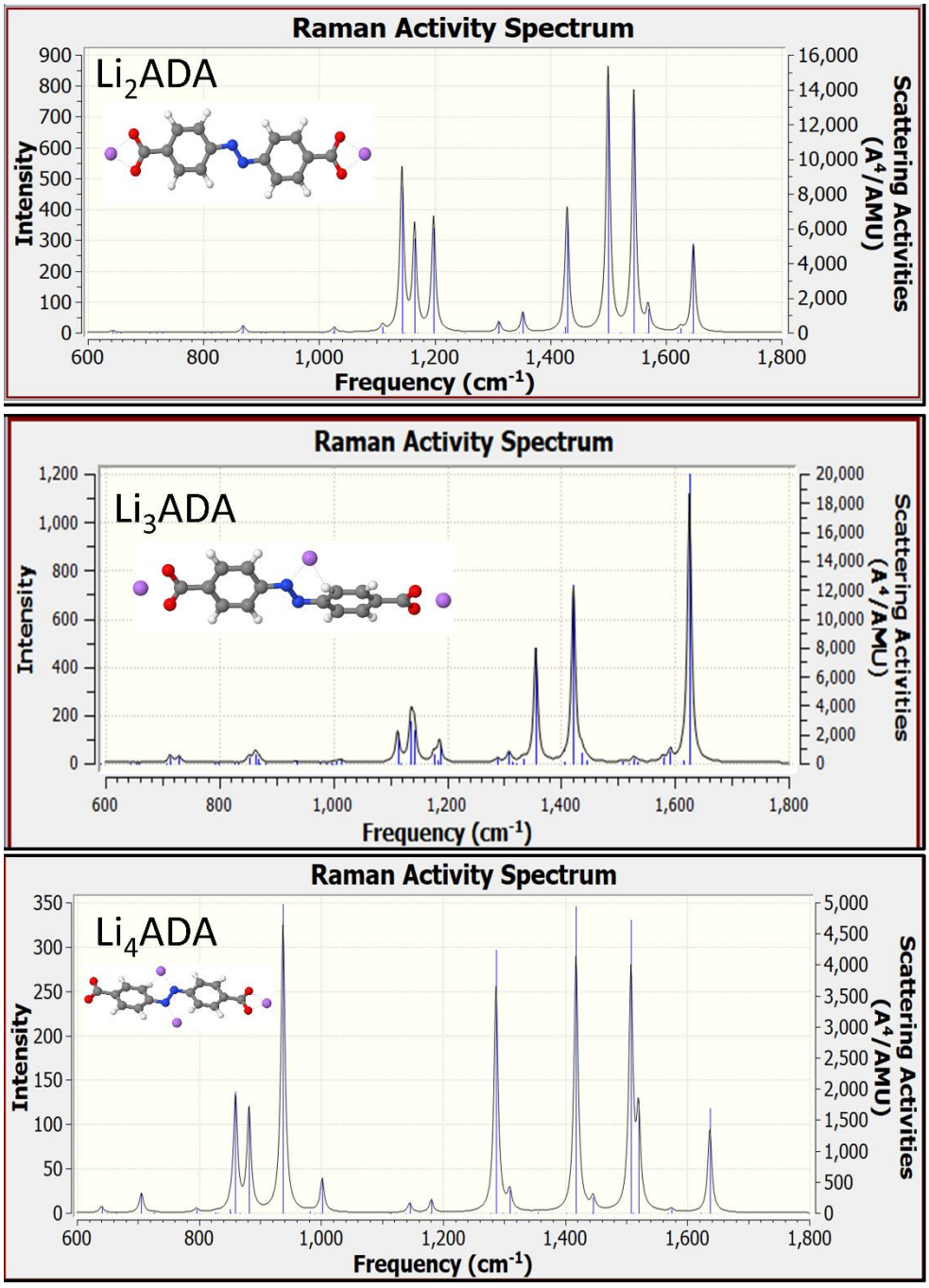

Fig. S12. Raman spectra from DFT calculations of Li_2ADA, Li_3ADA and Li_4ADA using B3LYP/aug-cc-pvTz/6-311G(d,p).

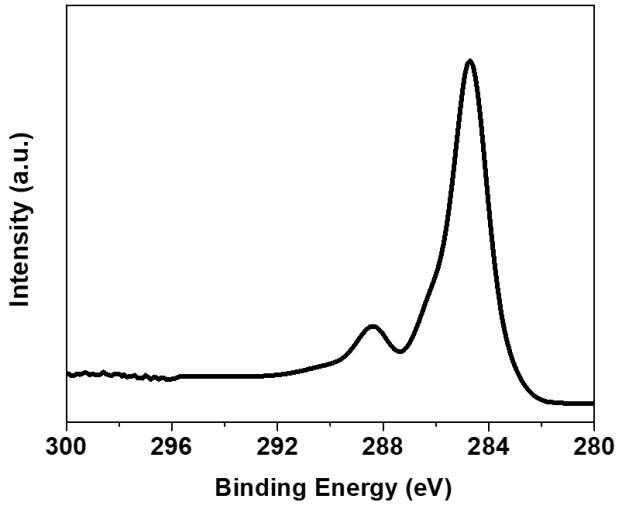

Fig. S13. XPS spectrum of ADALS electrode after 2 cycles at 1 V for C 1s.

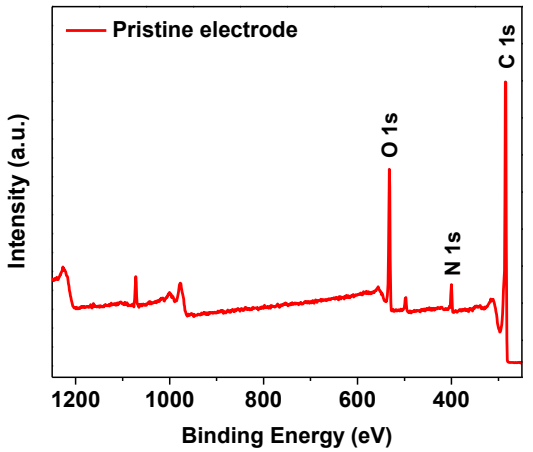

(a)

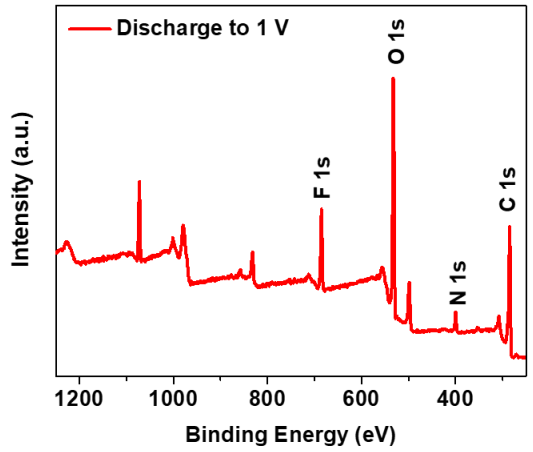

(b)

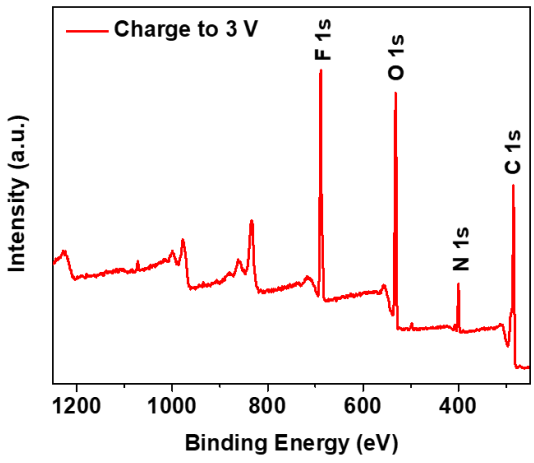

(c)

Fig. S14. XPS survey for (a) pristine electrode, (b) electrode discharged to 1 V and (c) electrode charged to 3 V after 2 cycles.

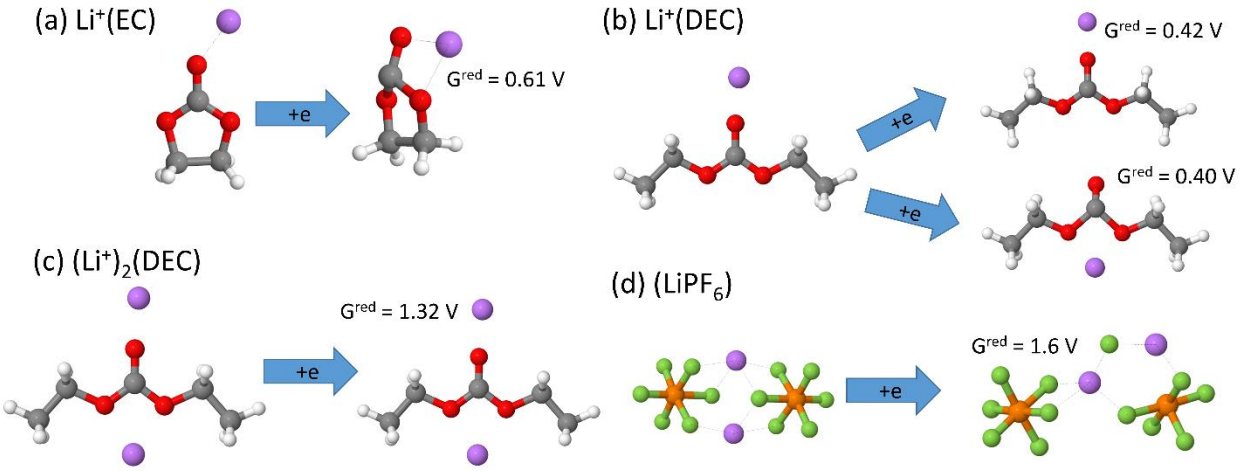

Fig. S15. Reduction potentials of the Li^+(EC) (a), Li^+(DEC) (b), $(Li_+)_2$(DEC) (c) and $(LiPF_6)_2$ (d) vs. Li/Li^+ surrounded by implicit solvent represented using SMD(ε=20) model from G4MP2 quantum chemistry calculations. The Li+(EC) and $(LiPF_6)_2$ reduction potentials were taken from previous work(24,25).

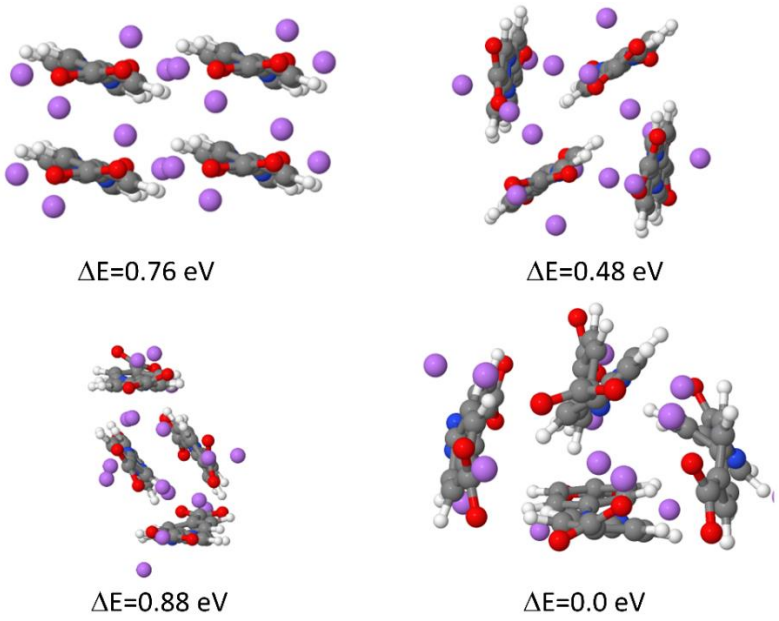

Fig. S16. Four optimized Li_4ADA periodic structures from DFT calculations performed using cp2k package and the associated relative energies per Li_4ADA.

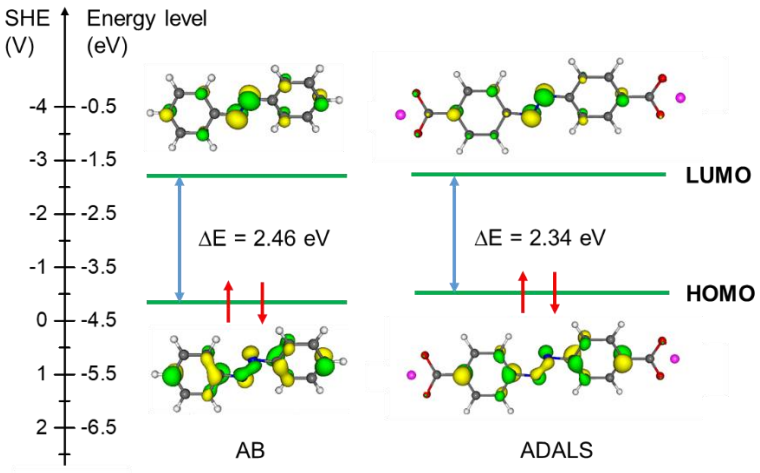

Fig. S17. DFT calculation results for the relative energies and optimized structures of AB and ADALS (The right axis aligns the relative energies in vacuum to the relative potential versus SHE).

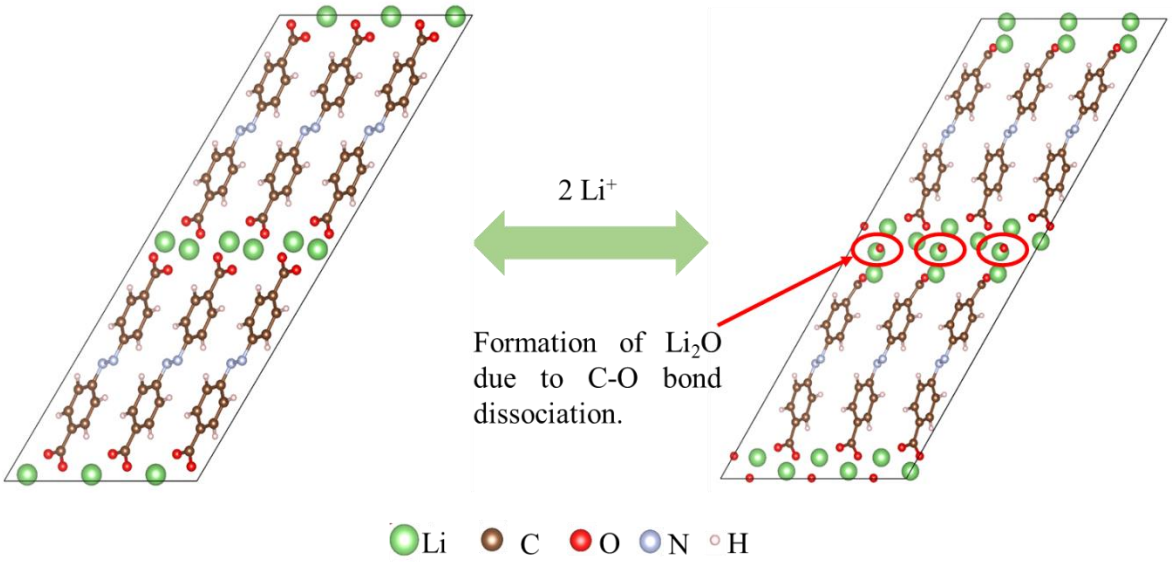

(a)

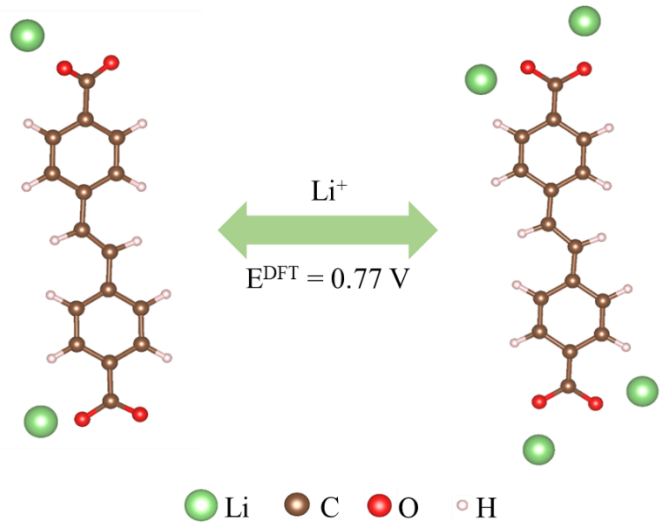

(b)

Fig. S18. (a) DFT calculation for the reduction of carbonyl groups in ADALS; (b) DFT calculation for the reduction of carbonyl groups in lithium 4,4′-stilbene-dicarboxylate.

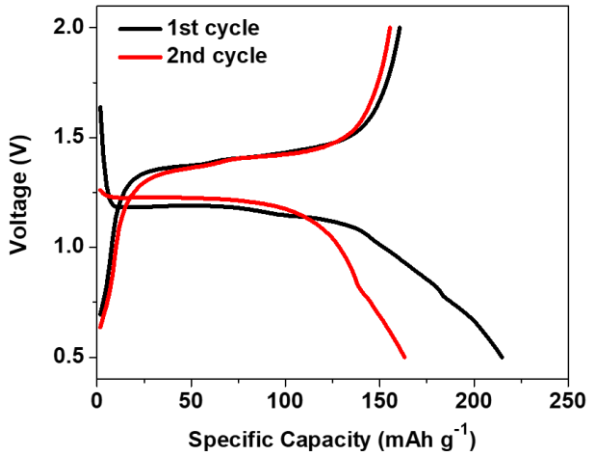

Fig. S19. The galvanostatic charge-discharge curves of ADASS at 1 C in Na-ion batteries.

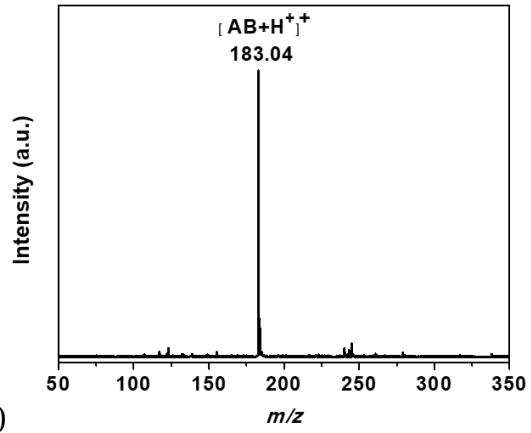

(a)

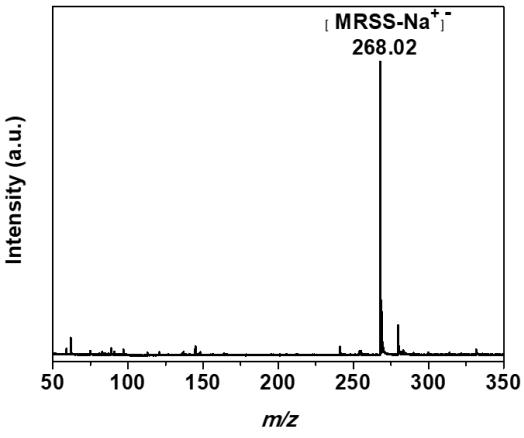

(b)

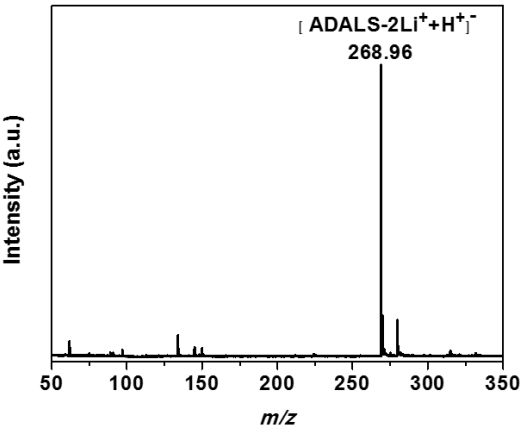

(c)

Fig. S20. Mass spectra for (a) AB, (b) MRSS and (c) ADALS.

References

1. M. J. Frisch et al. Gaussian I (2016) Gaussian 16, Revision A.03.
2. Frisch MJ, et al. (2010) Gaussian 09, Revision C1.
3. Zhao Y & Truhlar DG (2008) The M06 suite of density functionals for main group thermochemistry, thermochemical kinetics, noncovalent interactions, excited states, and transition elements: two new functionals and systematic testing of four M06-class functionals and 12 other functionals. Theor. Chem. Acc. 120(1-3): 215-241.
4. Barnes TA, Kaminski JW, Borodin O, & Miller TF (2015) Ab Initio Characterization of the Electrochemical Stability and Solvation Properties of Condensed-Phase Ethylene Carbonate and Dimethyl Carbonate Mixtures. J. Phys. Chem. C 119(8): 3865-3880.
5. Marenich AV, Cramer CJ, & Truhlar DG (2009) Universal Solvation Model Based on Solute Electron Density and on a Continuum Model of the Solvent Defined by the Bulk Dielectric Constant and Atomic Surface Tensions. J. Phys. Chem. B 113(18): 6378-6396.
6. Borodin O, Behl W, & Jow TR (2013) Oxidative Stability and Initial Decomposition Reactions of Carbonate, Sulfone, and Alkyl Phosphate-Based Electrolytes. J. Phys. Chem. C 117(17): 8661-8682.
7. Borodin O (2014) Molecular Modeling of Electrolytes. Electrolytes for Lithium and Lithium-Ion Batteries, Modern Aspects of Electrochemistry, eds Jow TR, Xu K, Borodin O, & Ue M (Springer New York), Vol 58, pp 371-401.
8. Lippert G, Hutter J, & Parrinello M (1997) A hybrid Gaussian and plane wave density functional scheme. Mol. Phys. 92(3): 477-487.

9. VandeVondele J, et al. (2005) QUICKSTEP: Fast and accurate density functional calculations using a mixed Gaussian and plane waves approach. Comput. Phys. Comm. 167(2): 103-128.
10. Goedecker S, Teter M, & Hutter J (1996) Separable dual-space Gaussian pseudopotentials. Phys. Rev. B 54(3): 1703-1710.
11. Hartwigsen C, Goedecker S, & Hutter J (1998) Relativistic separable dual-space Gaussian pseudopotentials from H to Rn. Phys. Rev. B 58(7): 3641-3662.
12. Grimme S, Antony J, Ehrlich S, & Krieg H (2010) A consistent and accurate ab initio parametrization of density functional dispersion correction (DFT-D) for the 94 elements H-Pu. J. Chem. Phys. 132(15): 154104.
13. Perdew JP, Burke K, & Ernzerhof M (1996) Generalized gradient approximation made simple. Phys. Rev. Lett. 77(18): 3865-3868.
14. Weber V, VandeVondele J, Hutter J, & Niklasson AMN (2008) Direct energy functional minimization under orthogonality constraints. J. Chem. Phys. 128(8): 084113.
15. Bussi G, Donadio D, & Parrinello M (2007) Canonical sampling through velocity rescaling. J. Chem. Phys. 126(1): 014101.
16. Hohenberg, P & Kohn, W (1964) Inhomogeneous electron gas. *Phys. Rev.* 136: B864-B871.
17. Kresse, G & Hafner, J (1994) *Ab initio* molecular-dynamics simulation of the liquid-metal—amorphous-semiconductor transition in germanium. *Phys. Rev. B: Condens. Matter Mater. Phys.* 49: 14251-14269.
18. Kohn, W & Sham, L.J (1965) Self-consistent equations including exchange and correlation effects. *Phys. Rev.* 140: A1133-A1138.

19. Blöchl, PE (1994) Projector augmented-wave method. *Phys. Rev. B: Condens. Matter Mater. Phys.* 50: 17953-17979.
20. Perdew, JP, Burke, K & Ernzerhof, M (1996) Generalized gradient approximation made simple. *Phys. Rev. Lett.* 77: 3865.
21. Kresse, G & Furthmüller, J (1996) Efficient iterative schemes for ab initio total-energy calculations using a plane-wave basis set. *Phys. Rev. B: Condens. Matter Mater. Phys.* 54: 11169-11186.
22. Jiang, D & Dai, S (2008) Circumacenes versus periacenes: HOMO–LUMO gap and transition from nonmagnetic to magnetic ground state with size. *Chem. Phys. Lett.* 466: 72-75.
23. Portmann, S & Lüthi, HP (2000) MOLEKEL: an interactive molecular graphics tool. *CHIMIA Int. J. Chem.* 54: 766-770.
24. Delp SA, et al. (2016) Importance of Reduction and Oxidation Stability of High Voltage Electrolytes and Additives. Electrochimica Acta 209: 498-510.
25. Borodin O, Olguin M, Spear CE, Leiter K, & Knap J (2015) Towards high throughput screening of electrochemical stability of battery electrolytes. Nanotechnology 26(35): 354003.